Noname manuscript No.
(will be inserted by the editor)

Millimeter-wave Enabled PAM-4 Data Transmission over Hybrid FSO-MMPOF Link for Access Networks

Saeed Iqbal · Aadil Raza · Muhammad Fasih Uddin Butt* · Jawad Mirza · Muhammad Iqbal · Salman Ghafoor · Mohammed El-Hajjar

Received: date / Accepted: date

Abstract In this paper, we propose a full duplex architecture based on a hybrid link composed of free space optics (FSO) and multimode plastic optical fiber (MMPOF) for short range wireless access networks. The proposed architecture employs mode group division multiplexing (MGDM) and wavelength reuse techniques to transmit data between central unit (CU) and radio access units (RAUs). An optical frequency comb source to generate multiple optical sidebands is realized by using a single laser source to provide 60 GHz millimeter-wave (mm-wave) signals at each RAU by simultaneously transmitting PAM-4 signal on linearly polarized (LP) modes of each optical sideband. Data rate of 2×12 Gbps at mm-wave frequency of 60 GHz is achieved for both downlink (DL) and uplink (UL) transmissions. The transmission of 2×12 Gbps PAM-4 signal over hybrid FSO-MMPOF link is investigated at different values of refractive index structure parameter (C_n^2) by employing

Saeed Iqbal
Department of Electrical and Computer Engineering, COMSATS University Islamabad, Islamabad, Pakistan
E-mail: saeed@biit.edu.pk

Aadil Raza
Department of Physics, COMSATS University Islamabad, Islamabad, Pakistan

* Muhammad Fasih Uddin Butt
Department of Electrical and Computer Engineering, COMSATS University Islamabad, Islamabad, Pakistan &
School of Electronics and Computer Science, University of Southampton, Southampton, United Kingdom

Jawad Mirza
SEECS, Photonics Research Group, Islamabad, Pakistan

Muhammad Iqbal
Department of Computer and Information Sciences, Pakistan Institute of Engineering and Applied Sciences (PIEAS), Islamabad, Pakistan

Salman Ghafoor
SEECS, National University of Sciences and Technology, Islamabad, Pakistan

Mohammed El-Hajjar
School of Electronics and Computer Science, University of Southampton, Southampton, United Kingdom

log-normal (LN) FSO channel model to support three RAUs in a ring topology. The acceptable receiver sensitivities below -5 dBm and -0.6 dBm for DL and UL transmissions are achieved, respectively. The proposed hybrid architecture can be a potential candidate for future communication networks.

Keywords Multimode plastic optical fiber · Free space optics · Mode group division multiplexing · Millimeter-wave · Pulse amplitude modulation

1 Introduction

Among the requirements of future communication networks is to provide higher data rate, improved performance as well as lower latency and ubiquitous services to the end users. Hence, in order to achieve these requirements, it is advantageous to exploit simultaneously both optical and wireless communication techniques. Optical fiber communication, despite having higher bandwidth and capacity, is not suitable for seamless coverage and mobility [1,2]. On the contrary, wireless communication provides better coverage and mobility, despite having limited radio frequency (RF) spectrum bandwidth resources and several sources of impairments [3]. To meet the unabated data rate demands, future communication networks can be an integration of optical and wireless communication technologies, which is referred to as radio over fiber (RoF) technology [4–6].

Furthermore, for the distribution of multiple wireless services for ultra-high bandwidth applications such as 3D and 4K videos in future communication networks, the fiber to the X (FTTX) technology has been adopted worldwide [7]. Here X in FTTX represents destinations, such as homes, buildings and premises and can therefore be termed as fiber to the home (FTTH), fiber to the building (FTTB) and fiber to the premises (FTTP), respectively. It has been reported in [7] that approximately 500 million FTTX connections have been deployed across the world till 2020 and this number is expected to grow further in the future. However, the deployment of FTTX networks in a congested residential or commercial areas involve large deployment cost of fiber. Generally, network providers opt for wireless signal transmission where they just need to install base station at different locations instead of digging the ground for laying fiber. Therefore, a potential solution would be free space optics (FSO) based solutions for backhaul high data rate transmission. FSO can provide increased capacity, immunity to electromagnetic interference and seamless transmission of high data rate optical signals at reduced installation and maintenance costs [8–11]. A hybrid link based on FSO and multimode plastic optical fiber (MMPOF) can be a potential solution for next generation wireless access networks because installation of FSO backhaul link is suitable in geographical areas such as hilly areas and canals, etc., where fiber cannot be deployed. MMPOF is more suitable for fronthaul links in indoor environments due to its larger core size as compared to single mode fiber (SMF). Although, SMF has advantages over MMPOF in terms of bandwidth, dispersion and attenuation but the installation cost of SMF and single mode transceivers is higher than MMPOF due to a need of trained people and high precision devices. In addition, MMPOF as compared to multimode glass optical fiber has smaller bending radius which makes

its installation comparatively easy [12,13]. In the literature, a hybrid link based architecture using 11 m FSO and 100 m MMPOF has been presented in [14] where the effects of fog and atmospheric turbulence for 11 m FSO link have been considered. In [15] the FSO link for different weather conditions has been investigated with passive optical network (PON) where different lengths of FSO channel with 25 km SMF has been achieved for 10 Gbps on-off keying (OOK) data rate. Additionally, duplex link of 50 km SMF and 100 m FSO has been reported in [16] to achieve 10 Gbps data rate. Furthermore, an FSO based FTTH network has been demonstrated by using 40 km SMF and 100 m FSO link to support 20/10 Gbps at 50/20 GHz millimeter-wave (mm-wave) communication [17].

Therefore, employing FSO for backhaul and MMPOF for fronthaul can provide a better solution for rural and urban areas. MMPOF is flexible, cheap and easy to handle hence it is attractive for in-building networks [6]. Furthermore, mode group division multiplexing (MGDM) in MMPOF by exploiting LP01 and LP11 modes provides additional degrees of freedom to achieve optical multiple input and multiple output (MIMO) transmission, which ultimately increases the throughput and number of users of the network [18,19]. To support higher data rates in access network, mm-wave communication can be used for the wireless link between the user equipment (UE) and the radio access unit (RAU). Modulation schemes like quadrature amplitude modulation (QAM), quadrature phase shift keying (QPSK) and pulse amplitude modulation-N (PAM-N), etc., have been used to achieve high throughput for mm-wave enabled RoF systems [20]. However, these higher order modulation schemes increase the complexity and cost of the system. On the contrary, PAM-N is implemented by utilising intensity modulation/direct detection (IM/DD), which is simple and cost efficient as compared to it's counterparts. Lately, PAM-4 has been standardized by IEEE P802.3bs 400 GbE task force owing to its lower power consumption, higher spectrum efficiency and inexpensive implementation [21–23].

To fulfill the requirements of future communication networks, a hybrid link based on MMPOF and FSO has been presented as a viable solution. The limitation of electronic techniques for the generation of mm-wave signals is solved by optical techniques such as heterodyne detection (HD). Additionally, the use of FSO link between central unit (CU) and residential gateway (RG) instead of the MMPOF further reduces the capital expenditure/operational expenditure (CAPEX/OPEX) while introducing extra mobility. The main objective in this work is to study the effects of integration of MMPOF and FSO on the system performance. The channel impairments of MMPOF and FSO can affect the system performance in such a way that the acceptable bit error ratio (BER) at the targeted forward error correction (FEC) limit is difficult to achieve. To solve this issue, we have optimized the data rates, MMPOF length, FSO link range and physical parameters of FSO transceiver in such a way that the BER at the targeted FEC limit is achieved successfully for both downlink (DL) and uplink (UL) transmissions. The system has enough robustness and resilience to the MMPOF and FSO impairments like, model crosstalk, atmospheric attenuation and turbulence etc.

In this paper, we demonstrate all-optical generation and transmission of mm-wave signals over hybrid FSO-MMPOF link, where MMPOF is used to connect

all RAUs in a ring architecture. Multiple optical carriers are generated by using a dual-drive Mach-Zehnder modulator (DDMZM) and a continuous wave (CW) laser source. Duplex transmission of 2×12 Gbps PAM-4 data signals between the CU and the RAUs over hybrid FSO-MMPOF link is achieved exploiting MGDM. Additionally, all-optical techniques are used to generate mm-wave signals for DL at the RAUs. While for the UL transmission, the received mm-wave signals at the RAUs from UEs are transmitted to the CU, after processing, using carrier reuse techniques. This simulation is performed in commercially available software: OptiSystem 17.

Based on the above discussion, the novel contributions of our work are summarized as follows:

1. The performance of the designed duplex PAM-4 based optical transmission system is analysed for a hybrid link of total length 600 m. This design is capable to support 60 GHz mm-wave services at throughput of 12 Gbps.
2. The FEC limit of BER at 3.8×10^{-3} is achieved for PAM-4 received signal for different values of refractive index structure parameter (C_n^2) of log-normal (LN) channel such as 5×10^{-16}, 5×10^{-15} and 5×10^{-14} $m^{-2/3}$ at lower receiver sensitivities.
3. We also show that an optical comb based upon a single laser source facilitates duplex transmission in all three RAUs simultaneously in a ring topology fashion. LP modes enabled mm-wave services are achieved at each RAU.

The rest of the paper is organised as follows. In Section 2, the proposed architecture is discussed in detail, where the generation of multiple optical carriers, the design and working of DL and UL transmission and receiver design for UE for mm-wave are presented. Then, the performance analysis and results are discussed in Section 3, while in Section 4, conclusions of this work are presented.

2 The Proposed Architecture

The proposed system based on hybrid FSO-MMPOF link is shown in Figure 1 where the RAUs are connected with the RG in a ring topology fashion using MMPOF, while the RG is connected to the CU using a FSO link. The CU is responsible for multi-wavelength generation, distribution and data modulation while each RAU performs photo-detection and amplification followed by the mm-wave signal transmission to the UE. At the CU, multi-wavelength signals are generated by using DDMZM and RF source having frequency of 30 GHz, which will be discussed in subsection 2.1. Six optical carriers λ_1, λ_2, λ_3, λ_4, λ_5, and λ_7 are separated using demultiplexer, as shown in Figure 2 for both the DL and the UL transmission which support three RAUs that are connected to the CU in a ring topology as shown in Figure 1. We use λ_7 instead of λ_6 to ensure the frequency separation of 60 GHz between λ_5 and λ_7 to generate 60 GHz mm-wave signal at the RAU-3. At the CU, optical MIMO is generated by passing each wavelength through mode generator to generate linearly polarized (LP) modes known as LP01 mode and LP11 mode of each wavelength, as shown in Figure 2. Data is modulated with λ_1, λ_2

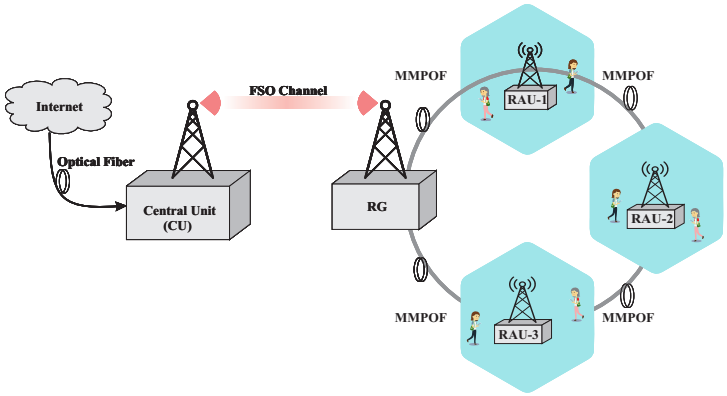

Fig. 1 Application scenario of the proposed architecture.

and λ_5 by using MZM for DL transmission toward RAU-1, RAU-2 and RAU-3, respectively, while λ_3, λ_4 and λ_7 are left as unmodulated carriers, which are used for UL transmission of RAU-1, RAU-2 and RAU-3, respectively. PAM-4 data is modulated with LP01 and LP11 mode of λ_1, λ_2 and λ_5 as shown in Figure 2. In Figure 2, the implementation detail for DL transmission to RAU-1 is shown while the DL transmissions for RAU-2 and RAU-3 are performed in a similar manner for RAU-1. Then, the multiplexed optical signal is transmitted over FSO link, where the FSO link has been modelled using LN FSO channel model [24]. After FSO transmission, the received optical signal is transmitted over MMPOF having length of 300 m. The simulation parameters of MMPOF are the same as the commercially available MMPOF having model number Giga-POF-50SR-Chromis Fiberoptics [18, 6]. The combined received optical signal is fed to a 1×8 spatial demultiplexer (DEMUX) to separate each carrier. Then the mm-wave signals are generated by HD and transmitted to the UE. Furthermore, the mm-wave signals received at RAUs from the UE are converted to optical signals and transmitted towards CU, which is discussed in subsection 2.2.

2.1 Downlink Transmission

The proposed model provides mm-wave services at high data rate to the end users, as shown in Figure 1. To facilitate multiple RAUs, multiple optical carriers are required at the CU to transport the data. Multiple laser sources can be used to achieve the required number of carriers. However, this increases the cost of the overall communication system. One of the possible solutions is to generate multiple optical carriers from a single laser source by exploiting the MZM properties which generate multiple sidebands when modulated by and an RF signal [25]. This can be achieved by modulating an RF signal with optical carrier of a single laser source, having peak wavelength of 1300 nm, by using a DDMZM, as shown in Figure 2.

It can be seen in Figure 2 that a laser diode (LD), an RF source of 30 GHz and a DDMZM are used to generate multiple side bands. The chirping effect is the inherit property of Mach-Zehnder modulator (MZM) which is exploited for generation of multiple optical carriers. Chirping effect is defined as the change in optical carrier's

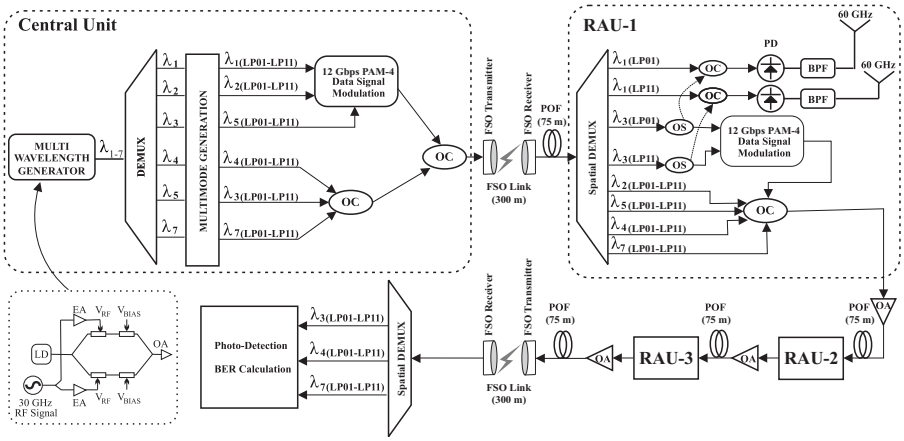

Fig. 2 The proposed architecture, **OS**: Optical splitter, **OA**: Optical amplifier, **OC**: Optical coupler, **FSO**: Free space optics, **BPF**: Bandpass filter, **PD**: Photodetector

phase at the output of the phase modulator (PM). The applied voltage to the branches of the DDMZM is controlled by electrical signal to produce the desire chirp which tends to change phase of optical signal passing through DDMZM [26]. This results into the generation of the multiple optical coherent carriers at the output of the DDMZM. The DDMZM is fed by the optical field of the LD which can be written as:

$$\zeta_{\mathrm{i}}(t) = \sqrt{P_{\mathrm{in}}}\exp(j2\pi f_{\mathrm{o}}t), \tag{1}$$

where f_{o} is frequency and P_{in} is the power of the optical carrier. The optical field at the output of the DDMZM is written as [27,28]

$$\zeta_{\mathrm{o}}(t) = \frac{\zeta_{\mathrm{i}}(t)}{2}\left[\exp\left\{j\frac{(1+\delta)\pi v_1(t)}{v_\pi}\right\} + \exp\left\{j\frac{(1-\delta)\pi v_2(t)}{v_\pi}\right\}\right]. \tag{2}$$

Where $v_1(t)$ and $v_2(t)$ are applied voltages to the upper and lower arms of the DDMZM, respectively. The 180$^{\mathrm{o}}$ change in phase is induced by v_π. The RF signals' applied voltage to DDMZM are selected as $v_2(t) = -v_1(t)$ to operate DDMZM in push-pull mode which is required to generate multiple side band of optical carrier. The RF signal applied to DDMZM is written as:

$$v_1(t) = \frac{1}{2}\left\{A_{\mathrm{rf}}\sin(\omega_{\mathrm{rf}}t) + A_{\mathrm{DC}}\right\}, \tag{3}$$

here A_{rf} and A_{DC} are the amplitude of the RF and DC bias voltage, respectively and

ω_{rf} is the RF signal's angular frequency. By putting Eq. (3) in Eq. (2) we get

$$\zeta_{\mathrm{o}}(t) = \frac{\zeta_{\mathrm{i}}(t)}{2}\left[\exp\left\{j\frac{(1+\delta)\pi(A_{\mathrm{rf}}\sin(\omega_{\mathrm{rf}}t)+A_{\mathrm{DC}})}{2v_\pi}\right\}\right. \\ \left.+\exp\left\{-j\frac{(1-\delta)\pi(A_{\mathrm{rf}}\sin(\omega_{\mathrm{rf}}t)+A_{\mathrm{DC}})}{2v_\pi}\right\}\right]. \tag{4}$$

$$\zeta_{\mathrm{o}}(t) = \frac{\zeta_{\mathrm{i}}(t)}{2}\left[\exp\{j\kappa_2\sin(\omega_{\mathrm{rf}}t)\}\exp(j\kappa_1)\right. \\ \left.+\exp\{-j\kappa_4\sin(\omega_{\mathrm{rf}}t)\}\exp(-j\kappa_3)\right]. \tag{5}$$

where

$$\kappa_1 = \frac{\pi(1+\delta)}{2v_\pi}A_{\mathrm{DC}}, \\ \kappa_2 = \frac{\pi(1+\delta)}{2v_\pi}A_{\mathrm{rf}}, \\ \kappa_3 = \frac{\pi(1-\delta)}{2v_\pi}A_{\mathrm{DC}}, \\ \kappa_4 = \frac{\pi(1-\delta)}{2v_\pi}A_{\mathrm{rf}}. \tag{6}$$

The operating point of the DDMZM is set at quadrature point so that intensity modulation is achieved. This mode of operation causes no distortion in the complete swing of the RF signal. Therefore, DC bias voltage is set as $v_\pi/2$, peak to peak modulation voltage is set equal to v_π and the peak voltage of RF signal A_{rf} is set equal to $v_\pi/2$. Therefore, by putting $A_{\mathrm{rf}} = A_{\mathrm{DC}} = v_\pi/2$ in Eq. (6), we get $\kappa_1 = \kappa_2$ and $\kappa_3 = \kappa_4 = \pi/2 - \kappa_1$. After substituting κ_2, κ_3 and κ_4 in terms of κ_1 in Eq. (5), the following equation is obtained

$$\zeta_{\mathrm{o}}(t) = \frac{\zeta_{\mathrm{i}}(t)}{2}\exp(j\kappa_1)\left[\exp\{j\kappa_1\sin(\omega_{\mathrm{rf}}t)\}\right. \\ \left.-j\exp\left\{(-j(\frac{\pi}{2}-\kappa_1)\sin(\omega_{\mathrm{rf}}t))\right\}\right]. \tag{7}$$

Finally, Eq. (7) can also be written as follows [29]

$$\zeta_{\mathrm{o}}(t) = \frac{\sqrt{P_{\mathrm{o}}}\exp(j\kappa_1)}{2}\left[\left\{J_{\mathrm{o}}(\kappa_1) - jJ_{\mathrm{o}}(\kappa_1 - \frac{\pi}{2})\right\}\exp(j2\pi f_{\mathrm{o}}t)\right.$$
$$+ \sum_{n=-\infty}^{\infty} J_{\mathrm{n}}(\kappa_1)\exp(j2\pi(f_{\mathrm{o}} + nf_{\mathrm{rf}})t) \tag{8}$$
$$\left. - j\sum_{n=-\infty}^{\infty} J_{\mathrm{n}}(\kappa_1 - \frac{\pi}{2})\exp(j2\pi(f_{\mathrm{o}} + nf_{\mathrm{rf}})t)\right].$$

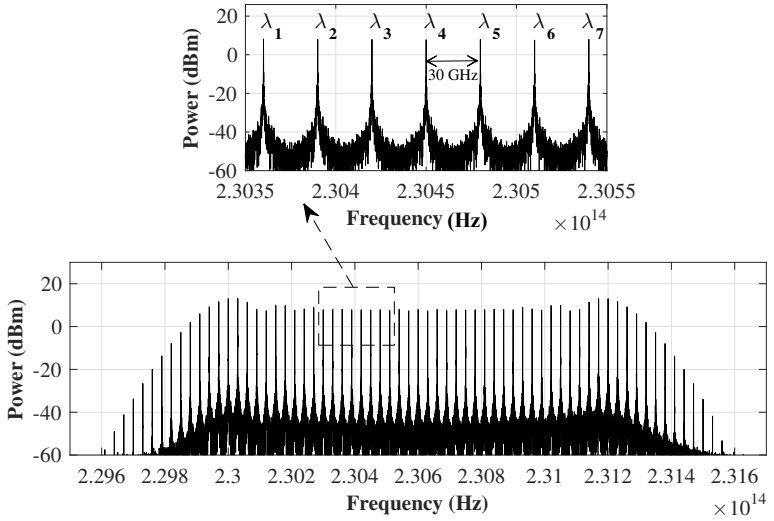

Fig. 3 Spectrum of generated multiple optical sidebands.

In above expression $J_{\mathrm{o}}(\kappa_1)$ and $J_{\mathrm{n}}(\kappa_1)$ are the Bessel functions of frequency (f_{o}) and n^{th} order, respectively. Here, n is the generated number of the sidebands. The spacing between the sidebands is controlled by the RF signal's frequency (f_{rf}) and hence in order to keep a 30 GHz frequency gap between sidebands, the frequency of the RF signal is chosen to be 30 GHz. Figure 3 shows multiple optical sidebands having sufficient power at the output of DDMZM which are generated by adjusting the biasing voltage and the amplitude of the RF signal as detailed in [6,18]. The proper selection of the sidebands will enable the generation of 60 GHz mm-wave signal at each RAU. The maximum power fluctuation among the sidebands is around 5 dBm as shown in Figure 3. Hence, any sideband can be used for data transmission. However, optical carriers λ_1, λ_2, λ_3, λ_4, λ_5 and λ_7 are chosen for the proposed architecture as a design example because all of these carriers have almost

the same power, as shown in Figure 3. Moreover, to perform HD at the RAUs to achieve mm-wave (60 GHz) transmission, the selection of optical carriers for DL and UL is made on the basis that there must be frequency difference of 60 GHz among them. Therefore, λ_1, λ_2, λ_5 are used for DL and λ_3, λ_4 and λ_7 are utilised for UL, as can be observed from Figure 2.

The signal at the output of DDMZM as shown in Figure 2 is fed into a 1×6 WDM-DEMUX to separate the six optical carriers having high optical signal to noise ratio (OSNR) which are at wavelengths λ_1, λ_2, λ_3, λ_4, λ_5 and λ_7, as shown in Figure 3. It may be noted that only these six wavelengths are selected specifically in the proposed system which are used both for DL and UL transmission. LP01 and LP11 modes of each wavelength are generated by using mode generator [18], as shown in Figure 2. For DL transmission, LP01 and LP11 mode of λ_1, λ_2 and λ_5, as shown in Figure 2, are intensity modulated with 12 Gbps PAM-4 signal using MZM. However, λ_3, λ_4 and λ_7 are left unmodulated to be used at the RAU for heterodyning and UL transmission and will be discussed in more detail in the next section. The modulated wavelengths (λ_1, λ_2, λ_5) and unmodulated wavelengths (λ_3, λ_4, λ_7) are multiplexed using WDM-MUX, as shown in Figure 2. The multiplexed signal at the output of WDM-MUX is then transmitted over FSO link with the help of FSO transmitter towards the RG, as shown in Figure 1. The transmitted signal undergoes various impairments of the FSO channel which include turbulence induced fading, atmospheric attenuation and polarization fluctuation effects [24,30]. The arbitrary fluctuation of the received intensity induced by the nonuniformities in atmospheric temperature and pressure is considered as prime contributor to signal degradation in the FSO link performance. Different channel models for FSO link have been reported in the literature [31]. The frequently employed FSO channel models are LN, K, Gamma-Gamma, negative exponential and Log normal-Rician models [31]. The LN channel model is used for weak turbulence in the case of clear weather conditions [32]. The variation in received signal intensity in LN channel model can be written by the following probability density function (PDF) [24,33]

$$p_I(I) = \frac{1}{2I\sqrt{2\pi\sigma_x^2}} exp\left[-\frac{\ln(I/I_o)^2}{8\sigma_x^2} \right]. \tag{9}$$

In above expression, I is the instantaneous light intensity, I_o is the instantaneous light intensity without turbulence and

$$\sigma_x^2 = 0.307 C_n^2 k^{7/6} L^{11/6}. \tag{10}$$

Here σ_x^2 is variance induced due to turbulence, C_n^2 is the refractive index structure parameter, L is the length of the FSO link in km and $k = 2\pi/\lambda$ is the wave number. Typically, the value of C_n^2 varies from 10^{-17} to 10^{-12} $m^{-2/3}$ for weak turbulence to strong turbulence, respectively [33]. After passing through hybrid LN based FSO-MMPOF channel, the received signals at the RAUs are processed to generate mm-wave signals which will then be transmitted to the UE. In the next section the processing at RAUs is discussed in more details.

2.2 Radio Access Unit

The RAUs are connected in a ring topology, as shown in Figure 1. The RAUs are responsible for generating mm-wave signals in the optical domain and then optical to electrical conversion is performed by using positive intrinsic negative (PIN) diode. After passing through a 75 m MMPOF, at RAU-1, a Spatial DEMUX is used to separate each wavelength and LP01 and LP11 modes, as shown in Figure 2. The design of mode filter embedded inside spatial DEMUX is realized by optimizing the interaction parameters of symmetric fiber couplers as demonstrated in [34]. The wavelength DEMUX used at each RAU has the following specifications. It has channel bandwidth of 0.75 $\times$ symbol rate = 0.75 $\times$ 6 GBaud = 4.5 GHz. Since the frequency separation between optical sidebands is 30 GHz and the channel bandwidth is 4.5 GHz, therefore there is an ignorable crosstalk between the DEMUX channels.

To generate mm-wave signal, LP01 mode of λ_1 which is modulated by PAM-4 signal and the unmodulated LP01 mode of λ_3 are given as an input to the optical coupler (OC) where the spacing between these wavelengths is 60 GHz. The combined optical signal at the output of the OC is given by the following expression

$$r(t) = aI(t)\Big[m(t)A_2\cos(2\pi f_1 t) + A_3\cos(2\pi f_3 t)\Big]. \tag{11}$$

Therefore, the intensity of the received optical signal can be written as

$$r(t) = aI(t)m(t)A_2\cos(2\pi f_1 t) + A_3\cos(2\pi f_3 t). \tag{12}$$

After square law photo-detection, the output current of the photodetector (PD) can be expressed as [35]

$$i_{PD}(t) = R\Big[r(t)\Big]^2, \tag{13}$$

$$\begin{aligned} i_{PD}(t) = R\Big[&A_2^2a^2I^2(t)m^2(t) + A_3^2 + A_2^2a^2I^2(t)m^2(t)\cos 2(\pi f_1 t) + \\ &A_3^2\cos 2\pi f_3 t + aI(t)m(t)A_2A_3\cos\big\{2\pi(f_1 - f_3)t\big\} + \\ &aI(t)A_2A_3m(t)\cos\big\{2\pi(f_1 + f_3)t\big\}\Big]. \end{aligned} \tag{14}$$

The double frequency terms ($f_1 + f_3$, $2f_1$ and $2f_3$) are at RF frequencies and can filtered using bandpass filter (BPF). Similarly, the DC terms are not transmitted by the antenna and are filtered before transmission. Hence leaving only the mm-wave term of interest which is transmitted over the wireless channel, as shown in Figure 2. Therefore, Eq. (14) reduces to

$$i_{PD}(t) = RaI(t)A_2A_3m(t)\cos\big\{2\pi(f_1 - f_3)t\big\}. \tag{15}$$

The beating of wavelengths results in the generation of mm-wave signal, which is obtained after passing the output of the PIN diode through BPF having center frequency at 60 GHz and bandwidth of 20 GHz. This BPF is used to pass only

mm-wave signal at 60 GHz frequency and stop all other noise like frequency components and then transmit to the UE.

At the UE, the received mm-wave signal is passed through a BPF to reject the out-of-band noise and then amplified using an electrical amplifier (EA). Self-mixing technique is used to down-convert the high frequency electronic signal to baseband signal which is then filtered out using lowpass filter (LPF) to obtain the baseband data signal [6]. In digital signal processing, least mean squared (LMS) algorithm is employed to mitigate the channel impairments.

RAU-1 receives mm-wave signals from the UE which are then modulated with LP11 and LP01 of λ_3 and are transmitted towards RAU-2 and then RAU-3 after coupling with other wavelengths λ_2, λ_4, λ_5 and λ_7 using MMPOF link, as shown in Figure 2. The optical signal further travels through 75 m and 150 m over MMPOF for RAU-2 and RAU-3, respectively. The optical signals received at RAU-2 and RAU-3 are treated in a similar manner as in RAU-1. The received mm-wave signals at RAU-1, RAU-2 and RAU-3 from the UE are processed before transmission toward the CU at the respective RAU as discussed in the next section.

2.3 Uplink Transmission

As shown in Figure 1, each RAU is responsible to provide coverage in a specific area where mm-wave signals are received at the RAU from the UE, as shown in Figure 1. At the RAU these signals are processed before transmission to the CU. For UL transmission, 60 GHz signal cannot be transmitted over MMPOF due to high losses at higher frequencies. Therefore, it may be noted that 12 Gbps PAM-4 data signal is realized at the RAU for UL transmission by self mixing of the 60 GHz mm-wave signal received from the UE. Then a LPF is used to filter out the PAM-4 signal which is shifted to baseband after self mixing. Then LP01 and LP11 modes of λ_3 at RAU-1 are re-used and modulated by 12 Gbps PAM-4 data signals using MZM, as shown in Figure 2. Both of the modulated optical signals are then combined with λ_2, λ_4, λ_5 and λ_7 by WDM-MUX and the combined optical signal at the output of WDM-MUX are transmitted towards RAU-2 and RAU-3 for UL transmission. Similarly, λ_4 and λ_7 are processed at RAU-2 and RAU-3, respectively as λ_3 is processed at RAU-1. At RAU-3 finally the modulated wavelengths λ_3, λ_4 and λ_7 are transmitted to the CU through hybrid FSO-MMPOF link. The multiplexed optical signal obtained at the CU is fed into 1×3 WDM-DEMUX to separate λ_3, λ_4 and λ_7, as shown in Figure 2, then MF is used to separate LP01 and LP11 modes of each received wavelength. Each mode, LP01 and LP11, of λ_3, λ_4 and λ_7 are treated independently to receive data of RAU-1, RAU-2 and RAU-3, respectively. LP01 and LP11 modes of each wavelength modulated by PAM-4 signal is then sent to photo-detection.

2.4 User Equipment

The received mm-wave signal is passed through a BPF for rejection of out-of-band noise and then amplified using an EA, as shown in Figure 4. Self-mixing technique is

used to down-convert the high frequency electronic signal to baseband signal which is then filtered out using Gaussian LPF to obtain the baseband data signal [6]. In digital signal processing (DSP), least mean squared (LMS) algorithm is employed to mitigate the channel impairments. Eventually, BER is calculated to analyse the system performance.

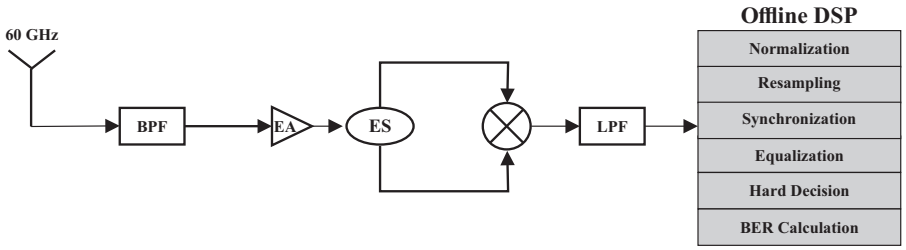

Fig. 4 Design of UE receiver for mm-wave. **LPF**: Lowpass filter, **ES**: Electrical splitter, **EA**: Electrical amplifier, **BPF**: Band pass filter.

Table 1 Simulation parameters

Data rate of PAM-4 signal	12 Gbps
Transmitter telescope diameter	5 cm
Receiver telescope diameter	20 cm
Beam divergence	2 mrad
Refractive index structure parameter	$5 \times (10^{-14}, 10^{-15}, 10^{-16})$ m $^{-2/3}$
Responsivity of PIN diodes	0.8 A/W
Optical amplifiers gain	20 dB
Optical amplifiers noise figure	4 dB

3 Performance Analysis

The performance of the proposed architecture is evaluated by analysing the bit error ratio (BER). Table 1 summarizes major simulation parameters used in our simulations. BER analysis is performed on the received PAM-4 signals. DSP techniques are used for offline processing of received PAM-4 signals. After normalization, PAM-4 signal is re-sampled [36]. Then, the equalisation is performed with the aid of pilot signal by using LMS algorithm for filter taps convergence. After the convergence the decision directed mode is enabled. Finally, the hard decision is performed to calculate BER. The power of the received optical signal at the RAUs is varied by using an optical attenuator to observe the effects on the BER. BER performance is analyzed on the basis of receiver sensitivity which is defined as the minimum received optical power (ROP) required to achieve BER of 3.8×10^{-3}. Figure 5 (a), (b), (c) show the BER versus ROP curves for RAU-1, RAU-2 and RAU-3 for DL transmissions while Figure 6 (a), (b), (c) show the BER versus ROP

curves for UL transmissions at different values of C_n^2. It may be observed from Figure 5 (a) that at $C_n^2 = 5 \times 10^{-16}$ m$^{-2/3}$, the receiver sensitivity at FEC limit of BER of 3.8×10^{-3}, for DL PAM-4 signal received at RAU-1 is around -12.5 dBm for LP01 and -10.8 dBm for LP11 as compared with that of RAU-2 and RAU-3 which are around -11.8 dBm for LP01, -9 dBm for LP11 and -10.2 dBm for LP01, -8.2 dBm for LP11, respectively. It can be seen from Figure 5 (a) that the receiver sensitivity of RAU-1 is lower than RAU-2 and RAU-3.

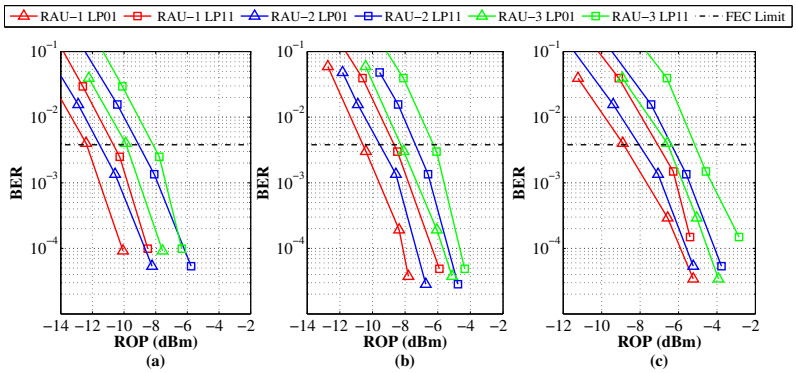

Fig. 5 BER versus received optical power for PAM-4 DL at (a): ($C_n^2 = 5 \times 10^{-16}$), (b): ($C_n^2 = 5 \times 10^{-15}$), (c): ($C_n^2 = 5 \times 10^{-14}$).

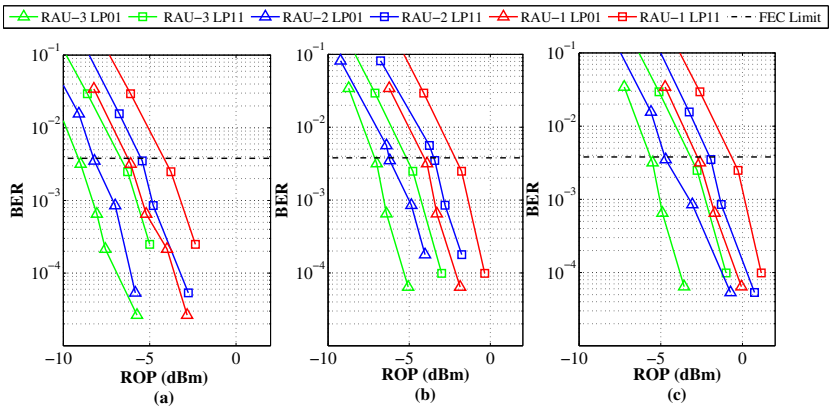

Fig. 6 BER versus received optical power for PAM-4 UL at (a): ($C_n^2 = 5 \times 10^{-16}$), (b): ($C_n^2 = 5 \times 10^{-15}$), (c): ($C_n^2 = 5 \times 10^{-14}$).

The reason for the variation in the receiver sensitivities among DL PAM-4 transmission may be understood from the spectral plot of optical carriers, as shown

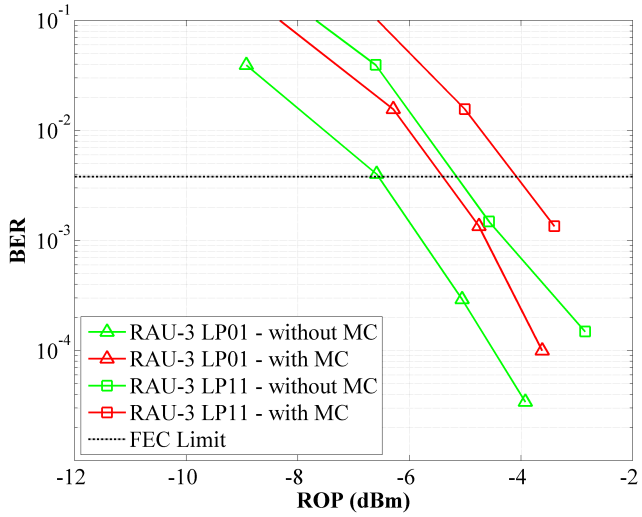

Fig. 7 BER versus received optical power at RAU-3 with and without mode coupling for $C_n^2 = 5 \times 10^{-14}$ m$^{-2/3}$.

in Figure 3. It can observed from Figure 3 that all wavelengths λ_1, λ_2, λ_3, λ_4, λ_5 and λ_7 have the same optical signal to noise ratio (OSNR). However, the reason for higher ROP of RAU-2 as compared to RAU-1 is due to the fact that the signal for RAU-2 has to travel longer distance than the signal for RAU-1 over MMPOF which results in higher degradation of the signal. The other reason may be polarization mode dispersion (PMD) and nonlinear effects of MMPOF. However, it is well known that PMD and nonlinear effects are limiting factors for long-haul optical transmission systems and at high transmitted laser's power, respectively [37,38]. However, in our work the power of the transmitted signal is lower for short rage communication therefore the aforementioned effects can be ignored. In addition, the large effective area of the MMPOF may also reduce the nonlinear effects and thus having no detrimental effects on signal quality. ROP at FEC limit of RAU-3 is higher because λ_5 has to travel longer distance to reach RAU-3 as compared to λ_1 and λ_2. Similarly, UL BER curves of PAM-4 data are shown in Figure 6 (a). It can be seen from Figure 6 (a) that FEC limit at RAU-3 is achieved at -9.1 dBm for LP01 and -6.9 dBm for LP11. FEC limit for RAU-2 and RAU-1 is achieved at -8.6 dBm for LP01, -5.2 dBm for LP11 and -6.6 dBm for LP01, -4.4 dBm for LP11, respectively. It can be seen in Figure 6 (a) that the FEC limit of BER for RAU-3 is achieved at lower ROP than RAU-1 and RAU-2 because of shorter distance over MMPOF is traveled by λ_7.

On increasing the value of C_n^2 parameter upto 5×10^{-15} m$^{-2/3}$, the minimum values of receiver sensitivities for DL PAM-4 signal received at RAU-3 are around -10.5 dBm for LP01 and -8.3 dBm for LP11, as shown in Figure 5 (b). FEC limit at RAU-2 is around -9.5 dBm for LP01 and -7.2 dBm for LP11 and at RAU-1 is around -8.2 dBm for LP01 and -6.3 dBm for LP11. Likewise, the minimum

receiver sensitivities for UL PAM-4 data at RAU-3 is −7.2 dBm for LP01 and −5.2 dBm for LP11, as presented in Figure 6 (b). FEC limit for RAU-2 and RAU-1 is achieved at −6.1 dBm for LP01, −3.8 dBm for LP11 and −3.8 dBm for LP01, −2.2 dBm for LP11, respectively.

Figure 5 (c) shows the DL received data's receiver sensitivities for $C_n^2 = 5 \times 10^{-14}$ m$^{-2/3}$. At RAU-1, ROP −9 dBm for LP01 and −7 dBm for LP11 are achieved while for RAU-2 and RAU-3 the values of ROPs are −8.2 dBm for LP01,−6.8 dBm for LP11 and −6.9 dBm for LP01, −5 dBm for LP11, respectively. Figure 6 (c) shows BER curves for UL transmission. It can observed from Figure 6 (c) that FEC limit at RAU-3 is achieved at −5.8 dBm for LP01 and −3.6 dBm for LP11. While at RAU-2 and RAU-1 FEC limit is achieved at −4.9 dBm for LP01, −2.8 dBm for LP11 and −2.2 dBm for LP01, −0.6 dBm for LP11, respectively. The reason behind this particular trend may be understood from the Eq. (10) which states that the variance of light intensity fluctuation can be increased by either increasing the length of FSO link or the value of C_n^2. By increasing the value of C_n^2, the variance increases which increases the BER which ultimately degrades the system performance. It may be noted that the results discussed so far are without the mode coupling effects commonly known as intra-model and inter-modal coupling in the fiber. Intra-mode coupling effect do not contribute significantly due to MGDM, so it can be ignored. However, inter-mode coupling always has a detrimental effect as compared to intra-mode coupling which obviously degrades the signal quality [39]. We observed around 1.2 dB penalty, after introducing crosstalk while keeping all other simulation parameters same, as shown in Figure 7 for the worst case scenario observed at RAU-3 for $C_n^2 = 5 \times 10^{-14}$ m$^{-2/3}$. In a nutshell, FEC limit of BER for both PAM-4 DL transmission is achieved at lower ROP for RAU-1 and for UL transmission it is achieved at lower ROP for RAU-3. It may be concluded from the results that the wavelengths of multi-wavelength comb can further be exploited by employing MGDM to increase the capacity of the hybrid FSO-MMPOF link. The length of FSO link and MMPOF between each RAU are appropriately selected to achieve BER in acceptable range for each channel.

4 Conclusion

A full duplex hybrid FSO-MMPOF architecture using ring topology is proposed for short range wireless access networks by employing MGDM and wavelength reuse techniques to transmit data between CU and RAUs. A comb of multiple sidebands is generated by using a single laser and RF source. LP01 and LP11 modes of each optical sideband are used to provide mm-wave services at each RAU by transmitting PAM-4 signals over hybrid FSO-MMPOF link. Data rate of 2×12 Gbps at 60 GHz is achieved at each RAU for both DL and UL transmissions by employing this cost effective hybrid FSO-MMPOF architecture. Wavelength reuse technique is used to achieve simplicity in terms of mm-wave generation by optical HD in RAUs to avoid the use of expensive RF local oscillators for mm-wave generation. The FEC limit, 3.8×10^{-3}, for PAM-4 signal is achieved for weak turbulence at ROP −11.5 dBm,

−10.8 dBm and −9.2 dBm for RAU-1, RAU-2 and RAU-3, respectively. The proposed architecture is capable of providing better coverage and enhance data rate with better BER performance.

Conflict of interest

On behalf of all authors, the corresponding author states that there is no conflict of interest.

References

1. F.J. Leonberger, H. Melchior, R.M. Osgood, Y. Yoshikuni, IEEE Journal of Selected Topics in Quantum Electronics **6**(1), 1 (2000)
2. M.Z. Chowdhury, M.K. Hasan, M. Shahjalal, M.T. Hossan, Y.M. Jang, IEEE Communications Surveys Tutorials **22**(2), 930 (2020). DOI 10.1109/COMST.2020.2966855
3. A. Goldsmith, *Wireless Communications* (Cambridge University Press, 2005)
4. V.A. Thomas, S. Ghafoor, M. El-Hajjar, L. Hanzo, IEEE Microwave Magazine **16**(9), 64 (2015)
5. V.A. Thomas, M. El-Hajjar, L. Hanzo, IEEE Communications Surveys Tutorials **17**(2), 627 (2015)
6. A. Raza, S. Ghafoor, M.F.U. Butt, Photonic Network Communication **35**(2), 265 (2018)
7. [online] Available: https://www.marketresearch. com/product/sample-8281254.pdf. ([Accessed 7-9-2019])
8. M. Z. Chowdhury, M. K. Hasan, M. Shahjalal, E. B. Shin and Y. M. Jang, (International Conference on Artificial Intelligence in Information and Communication (ICAIIC), 2019), pp. 004–007
9. H. Willebrand, B.S. Ghuman, *Free space optics: enabling optical connectivity in today's networks* (SAMS publishing, 2002)
10. R. Miglani, M. Singh, IEEE (Fiber Optics in Access Network (FOAN), 4th International Workshop on, 2013), pp. 31–35
11. Y. Liu, H. Li, Optical Review **26**, 303 (2019)
12. M. Li, in *OFC 2014* (2014), pp. 1–3
13. S. Iqbal, M. Iqbal, A. Raza, J. Mirza, S. Ghafoor, M. El-Hajjar, M.F.U. Butt, Electronic Letters **56**(21), 1125 (2020)
14. H.K. Al-Musawi, T. Cseh, M.M. Abadi, W.P. Ng, Z. Ghassemlooy, E. Udvary, T. Berceli, (17th International Conference on Transparent Optical Networks (ICTON), 2015), pp. 1–4
15. C.H. Yeh, C.S. Gu, B.S. Guo, Y.J. Chang, C.W. Chow, M.C. Tseng, R.B. Chen, Journal of Optics (2018)
16. X.H. Huang, H.H. Lu, S. Donati, C.Y. Li, Y.C. Wang, Y.B. Jheng, J.C. Chang, Laser Physics (2018)
17. C. Li, H. Lu, W. Tsai, X. Huang, Y. Wang, Y. Chen, Y. Wu, IEEE Photonics Journal **10**(2), 1 (2018)
18. S. Iqbal, A. Raza, M. Fasih Uddin Butt, S. Ghafoor, M. El-Hajjar, Transactions on Emerging Telecommunications Technologies **e3910** (2020)
19. I. Chatti, F. Baklouti, F. Chekir, R. Attia, Optical Review **26**, 631 (2019)
20. J. Beas, G. Castanon, I. Aldaya, A. Aragon-Zavala, G. Campuzano, IEEE Communications Surveys Tutorials **15**(4), 1593 (2013)
21. K. Zhong, X. Zhou, T. Gui, L. Tao, Y. Gao, W. Chen, J. Man, L. Zeng, A.P.T. Lau, C. Lu, Opt. Express **23**(2), 1176 (2015)
22. [online] Available: http://www.ieee802.org/3/bs/ ([Accessed 15-12-2019])
23. A. Raza, K. Zhong, S. Ghafoor, S. Iqbal, M. Adeel, S. Habib, M.F.U. Butt, C. Lu, Chin. Opt. Lett. **16**(4), 040604 (2018). URL http://col.osa.org/abstract.cfm?URI=col-16-4-040604
24. J. Mirza, S. Ghafoor, A. Hussain, Microwave and Optical Technology Letters (2020)
25. J. K. Hmood, S. D. Emami, K. A. Noordin, H. Ahmad, S. W.Harun and H. M. H. Shalaby, Optics Communications **344**, 139 (2015). DOI 10.1109/LPT.2005.853035
26. L. Zhang, Y. Song, S. Zou, Y. Li, J. Ye, R. Lin, (IEEE 12th International Conference on Communication Technology, 2010), pp. 211–213
27. F. Koyama, K. Iga, Journal of Lightwave Technology **6**(1), 87 (1988)
28. K.P. Ho, J.M. Kahn, Journal of Lightwave Technology **22**(2), 658 (2004)

29. B.G. Korenev, *Bessel Functions and Their Applications* (CRC Press, 2002)
30. J. Mirza, S. Ghafoor, A. Hussain, Optical Engineering **58**(5), 056103 (2019)
31. L.C. Andrews, R.L. Phillips, *Laser beam propagation through random media*, vol. 152 (SPIE press Bellingham, WA, 2005)
32. E.J. Lee, V.W. Chan, IEEE Journal on Selected Areas in Communications **22**(9), 1896 (2004)
33. K. Davaslog lu, E. Cagiral, M. Koca, Optics express **18**(16), 16618 (2010)
34. N. Hanzawa, K. Saitoh, T. Sakamoto, T. Matsui, S. Tomita, M. Koshiba, in *2011 Optical Fiber Communication Conference and Exposition and the National Fiber Optic Engineers Conference* (2011), pp. 1–3
35. J.A. Nanzer, P.T. Callahan, M.L. Dennis, T.R. Clark Jr, Johns Hopkins APL Technical Digest **30**(4), 299 (2012)
36. M. Chagnon, M. Osman, M. Poulin, C. Latrasse, J.F. Gagné, Y. Painchaud, C. Paquet, S. Lessard, D. Plant, Opt. Express **22**(17), 21018 (2014)
37. M. Li, X. Chen, D.A. Nolan, in *Optical Fiber Communication Conference, 2004. OFC 2004*, vol. 2 (2004), vol. 2, p. 3
38. N. Bloembergen, IEEE Journal of Selected Topics in Quantum Electronics **6**(6), 876 (2000)
39. M. Awad, I. Dayoub, A. Okassa MFoubat, J. M. Rouvaen, Optics Communications **282**(19), 3908 (2009)